Dynamical Effects of Cold Dark Matter Subhalos on a Galactic Disk

PASJ: Publ. Astron. Soc. Japan **58**, 835–846, 2006 October 25

Dynamical Effects of Cold Dark Matter Subhalos on a Galactic Disk

Hirohito HAYASHI and Masashi CHIBA
Astronomical Institute, Tohoku University, Sendai 980-8578
hayashi@astr.tohoku.ac.jp, chiba@astr.tohoku.ac.jp

(Received 2006 May 11; accepted 2006 August 28)

Abstract

We have investigated the dynamical interaction between a galactic disk and numerous surrounding dark subhalos as expected for a galaxy-sized halo in the cold dark matter models. Our particular interest is to what extent accretion events of subhalos into a disk are allowed in light of the observed thinness of a disk. Several models of subhalos were considered in terms of their internal density distribution, mass function, and spatial and velocity distributions. Based on a series of N-body simulations, we find that disk thickening, quantified by the change of its scale height, $\Delta z_{\rm d}$, depends strongly on the individual mass of an interacting subhalo, $M_{\rm sub}$. This is described by the relation $\Delta z_{\rm d}/R_{\rm d} \simeq 8\sum_{j=1}^{N}(M_{{\rm sub},j}/M_{\rm d})^2$, where $R_{\rm d}$ is the disk scale length, $M_{\rm d}$ is the disk mass, and N is the total number of accretion events of subhalos inside a disk region ($\leq 3\,R_{\rm d}$). Using this relation, we find that an observed thin disk has never interacted with subhalos with a total mass of more than 15% of the disk mass. Also, a less-massive disk with a smaller circular velocity, $V_{\rm c}$ is more affected by subhalos than a disk with a larger $V_{\rm c}$, in agreement with observations. Further implications of our results for the origin of a thick disk component are also discussed.

Key words: cosmology: dark matter — galaxies: formation — galaxies: interactions — galaxies: structure

1. Introduction

The cold dark matter (CDM) paradigm has become a standard framework for understanding structure formation in the Universe. According to this theoretical paradigm, the growing process of self-gravitating structures is hierarchical in the sense that small dark-matter halos virialize first, and aggregate successively into larger and larger objects. This clustering process of dark-matter halos is successful for explaining a wide variety of observations, including the large-scale distribution of galaxies.

In this CDM scenario, N-body simulations are an important tool to investigate the non-linear growth of cosmological structures. Early N-body simulations based on the CDM models suffered from the so-called over-merging problem, i.e., substructures are disrupted very quickly within dense environments (Summers et al. 1995). However, recent high-resolution N-body simulations have revealed the presence of hundreds of dark-matter substructures (subhalos) that survive on not only cluster scales, but also on galactic scales (Moore et al. 1999; Klypin et al. 1999). This large number of subhalos in a galaxy-sized halo is in contrast to only about a dozen satellite galaxies in the Galaxy, which confronts the so-called the Missing Satellite Problem. Several authors have argued that this apparent discrepancy could be resolved by considering some suppressing process for star formation, such as gas heating by an intergalactic ionizing background, or energy feedback from evolving stars. In whatever models relying on the suppression of galaxy formation, a typical galaxy-sized halo should contain numerous dark subhalos.

Then, there is a possibility that a large number of subhalos interact frequently with a stellar disk embedded at the center of a halo, so that the disk would be dynamically heated and thickened. On the other hand, an observed galactic disk is rather thin; the scale height (or half thickness) is only about $\sim 250\,$pc in the Galaxy. Likewise, recent observations of external disk galaxies (Kregel et al. 2002) suggest that the observed scale height of a disk, $z_{\rm d}$, is confined to some limiting value relative to the scale length of a disk, $R_{\rm d}$, i.e., $z_{\rm d}/R_{\rm d} < 0.2$.

This observed thinness of a disk provides important limits on disk heating due to infalling satellites. Tóth and Ostriker (1992) analytically evaluated this effect and concluded that an observed disk like that of the Galaxy within the solar radius should have interacted with satellites with no more than 4% of the present disk mass within the last 5 Gyr. Subsequent numerical simulations of an interaction between a disk and a single satellite (e.g. Velázquez, White 1999) showed that their analytical estimation for disk heating was somewhat too high because an actual interaction process is highly non-linear and more complicated than a simplified analytical representation. Interactions with many subhalos would be much more complicated, and thus require a more detailed analysis.

Font et al. (2001) have conducted numerical simulations of interactions between a disk and numerous subhalos based on the CDM models. They concluded that the effect of subhalos on a disk is rather small, and therefore subhalos do not conflict with the presence of a thin disk, since their orbit seldom take them near the disk. However, it is worth noting that in their simulation the initial scale height of a disk (700 pc) was already thick compared with the observed one in the Galaxy ($\sim 250\,$pc), thereby leading to a possibly underestimating the disk-heating effect. Their simulation was also limited to only one realization of subhalos; it is yet unclear whether the derived weak effect of subhalos on a disk is general or not. Ardi et al. (2003) have investigated more details in this disk heating by subhalos. They found that a more massive subhalo is more effective to heat the disk than a less massive one. However, in their calculation subhalos were represented by rigid bodies that never lose

their mass, irrespective of tidal effects of a host galaxy, so that the disk heating was overestimated. Also, the applicability of their result to an actual disk, especially, to what extent accretion events of subhalos into a disk are allowed, remains unclear.

Our aim of the present work was thus to set more useful limits on the dynamical interaction between numerous subhalos and a galactic disk. For this purpose, we conducted a series of numerical simulations, in which a self-gravitating disk was embedded in a dark halo containing many subhalos. In this work we set an initially thin disk with a scale height of 250 pc, in contrast to previous numerical studies starting from a scale height of ~ 700 pc, much larger than the observed one (Velázquez, White 1999; Font et al. 2001). Several models for the system of subhalos in a host halo were taken into account in terms of their mass function, spatial distribution, and velocity distribution. We also considered two different models for the internal density distribution of subhalos: point-mass and extended-mass models. In the latter model, subhalos are affected by a tidal field of a host galaxy, so that they lose their mass during the course of their orbital motions. Based on our simulations, we investigated the dependence of the disk heating on the model parameters and applied our analysis to understanding an observed thin disk in the context of disk heating by subhalos.

This paper is organized as follows. In section 2 we describe our galaxy model, which is composed of halo, bulge, and disk components. The models of subhalos are also described in this section. In section 3 we present the results of our numerical simulations. In section 4 we analyze our results and present our prediction for the relation between the disk heating by subhalos and an observed thin or thick disk. Finally, in section 5 we present our conclusions.

2. Models

2.1. The Galaxy Model

Our galaxy model is composed of three components: a disk, a bulge, and a dark halo. To investigate the self-gravitating response of the disk component to orbiting subhalos, we modeled the disk by a self-consistent N-body realization of stars under the influence of an external force provided by the rigid bulge and halo components. The methods of Hernquist (1993) were utilized to set up a disk consisting of a distribution of N-body particles. A detailed description of the technique can be found in Hernquist's paper.

The density distribution of the disk is initially axisymmetric, $\rho_{\rm d}(R, z)$, using cylindrical coordinates (R, z), while the bulge and halo are spherically symmetric, $\rho_{\rm b}(r)$ and $\rho_{\rm h}(r)$, respectively, using the galactocentric distance, r. These density distributions are given by

$$\rho_{\rm d}(R,z) = \frac{M_{\rm d}}{4\pi R_{\rm d}^2 z_{\rm d}} \exp(-R/R_{\rm d}) \,{\rm sech}^2(z/z_{\rm d}), \tag{1}$$

$$\rho_{\rm b}(r) = \frac{M_{\rm b}}{2\pi} \frac{a_{\rm b}}{r(a_{\rm b}+r)^3}, \tag{2}$$

$$\rho_{\rm h}(r) = \frac{M_{\rm h}}{2\pi^{3/2}} \frac{\alpha_{\rm h}}{r_{\rm c}} \frac{\exp(-r^2/r_{\rm c}^2)}{r^2+\gamma^2}, \tag{3}$$

Table 1. Galactic parameters.

	Symbol	Value
Disk:		
	N_d*	46000
	$M_{\rm d}$	$5.6 \times 10^{10}\,M_\odot$
	$R_{\rm d}$	3.5 kpc
	$z_{\rm d}$	245 pc
	$Q_\odot$	1.5
	$R_\odot$	8.5 kpc
	ϵ	70 pc
Bulge:		
	$M_{\rm b}$	$1.87 \times 10^{10}\,M_\odot$
	$a_{\rm b}$	525 pc
Halo:		
	$M_{\rm h}$	$7.84 \times 10^{11}\,M_\odot$
	γ	3.5 kpc
	$r_{\rm c}$	84 kpc

* The number of particles used for the disk.

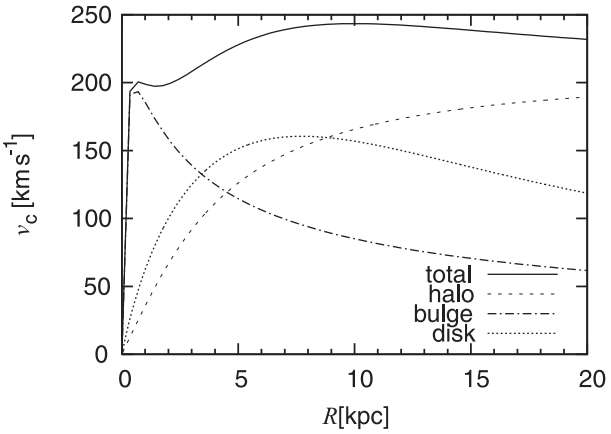

Fig. 1. Rotation curves for our disk galaxy model.

where $M_{\rm d}$, $M_{\rm b}$, and $M_{\rm h}$ correspond to the masses of the disk, the bulge, and the halo, respectively. The disk parameters, $R_{\rm d}$ and $z_{\rm d}$, denote the radial scale length and vertical scale height, respectively. The parameter $a_{\rm b}$ denotes the scale length of the bulge, while γ and $r_{\rm c}$ are the core and cut-off radii for the halo and $\alpha_{\rm h}$ is a normalization constant. We chose these parameters so that the model would approximately match the observed characteristics of the Galaxy; the values of the parameters are listed in table 1. It is worth remarking that we considered an observed thin scale height for the disk, namely $z_{\rm d} = 245$ pc, in contrast to the models by Font et al. (2001) and Velázquez and White (1999), adopting $z_{\rm d} = 700$ pc. In order to prevent the disk from gravitational instability, we adopted a stable disk by setting Toomre's Q parameter at the solar radius $R_\odot = 8.5$ kpc as $Q_\odot = 1.5$. The rotation curve of our galaxy model is shown in figure 1. The rotation speed at the solar radius was $V_{\rm c}(R_\odot) \approx 240\,{\rm km\,s^{-1}}$.

Table 2. The parameters of the subhalo models.

Model	Number of subhalos	a [kpc]	$M_{\rm high}$ [$M_\odot$]	$M_{\rm low}$ [$M_\odot$]	$n_{\rm sub}$*
point-mass models with $\beta = 0$					
A	784	70	10^8	10^8	
B	784	140	10^8	10^8	
C	392	140	2×10^8	2×10^8	
D	261	140	3×10^8	3×10^8	
E	200	175	4×10^8	4×10^8	
F	318	87.5	10^9	10^8	
G	313	280	10^9	10^8	
H	175	140	10^{10}	10^8	
I	1141	175	10^{10}	10^7	
J	1959	140	10^9	10^7	
extended-mass models with $\beta = 0$					
K	318	87.5	10^9	10^8	182
L	175	140	10^{10}	10^8	182
M	362	24.5	10^9	10^8	182
N	200	175	4×10^8	4×10^8	182
O	112	70	7×10^8	7×10^8	182
P†	280	52.5	10^{10}	10^8	170
Q	173	24.5	10^{10}	10^8	170
point-mass models with $\beta = 0.5$					
R	197	140	10^{10}	10^8	
S	362	87.5	10^9	10^8	
T	249	140	3×10^9	10^8	
U	361	157.5	10^9	10^8	

* The number of particles used for each subhalo.
† Only in this model, the total mass of the subhalo system is 13% of that of the host galaxy.

2.2. *Subhalo Models*

We constructed a set of subhalo models in our numerical simulations, designated as models A to U, as tabulated in table 2, to investigate how different physical properties of subhalos affect the disk heating process. Each model assumption is explained as follows.

2.2.1. *Mass function, spatial distribution, and velocity anisotropy*

We considered a mass spectrum for the realization of each subhalo with a mass $M_{\rm sub}$. According to the results of cosmological N-body simulations by Moore et al. (1999), Klypin et al. (1999), and Ghigna et al. (2000), this mass function can be fitted to a power law with an index of about -2. We thus adopted the form

$$N(M_{\rm sub})\, dM_{\rm sub} \propto M_{\rm sub}^{-2}\, dM_{\rm sub}. \tag{4}$$

For the convenience of numerical analysis, we set the higher and lower mass limits for this mass function designated as $M_{\rm high}$ and $M_{\rm low}$, respectively, and examined the role of individual subhalo masses in the disk heating. The normalization of proportionality (4) is given by the total mass of the subhalo system, which is about one-tenth of the mass of a host halo according to Klypin et al. (1999) and Ghigna et al. (2000). We thus set $0.1\, M_{\rm h}$ as the total mass of the subhalo system.

Recent high-resolution N-body simulations have shown that the spatial distribution of subhalos in a host halo is less concentrated than the host's density profile (Gao et al. 2004), which is often represented by the so-called NFW profile (Navarro et al. 1997). However, in even most recent simulations the mass and force resolutions are yet insufficient, so the true spatial distribution of subhalos is unclear. In the present work, instead of trying to set a realistic spatial distribution (which is yet unknown), we adopted a tractable model for it and attempted to extract general results that do not depend on this particular setting. Thus, for the initial spatial distribution of subhalos in a host halo, we adopted the Hernquist model (Hernquist 1990), in which the number density $n(r)$ of subhalos at the galactocentric distance r is given as

$$n(r) \propto \frac{1}{r(a + r)^3}, \tag{5}$$

where a is the scale length in the spatial distribution. It is worth noting that the inner density distribution of this model is similar to that of the NFW profile. The change of the parameter a affects the incidence of subhalo–disk interaction, which is mostly effective at $r \lesssim 10\,$kpc, since a smaller a yields smaller pericenters and apocenters for the orbits of subhalos.

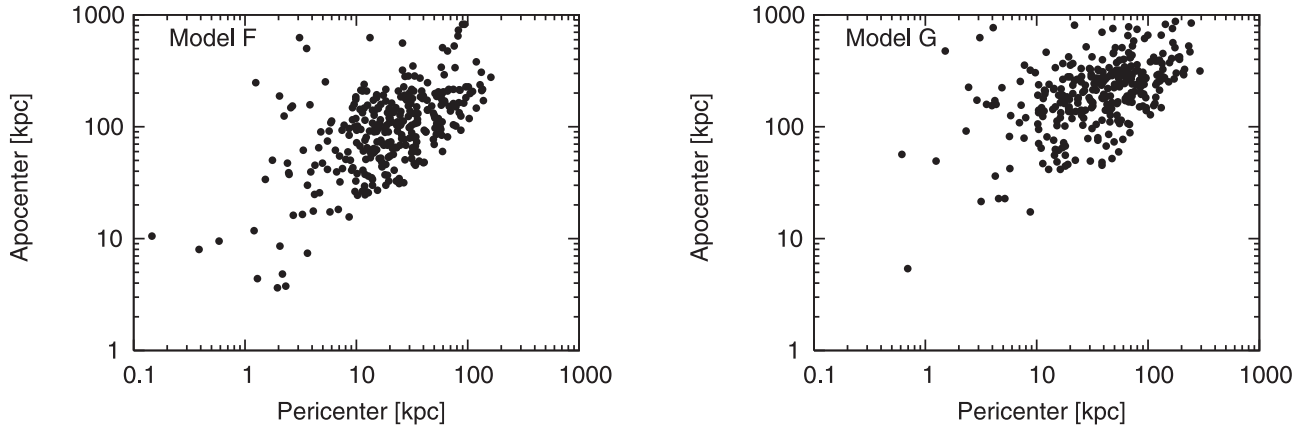

Fig. 2. Distributions of the pericenter and the apocenter of the subhalos in Model F (left panel) and Model G (right panel).

This is highlighted in figure 2, where the distributions of the pericenters and apocenters of subhalos are shown for Model F ($a = 87.5$ kpc) and Model G ($a = 280$ kpc), while having the same velocity distribution (see below). It follows that the number of subhalos orbiting interior to $r = 10$ kpc is larger for Model F than for Model G, and the dependence of this number on the scale length, a, is also seen in other models.

For the initial velocity distribution of subhalos, we took the moments of the collisionless Boltzmann equation following a procedure described by Hernquist (1993). The velocity ellipsoid at each spatial location was calculated from the moment equations, and then the velocity components were randomly selected from the Gaussian distributions for the corresponding velocity ellipsoid.

We adopted two different models for the velocity anisotropy of the subhalo system, which is parameterized by $\beta \equiv 1 - 0.5(\sigma_\theta^2 + \sigma_\phi^2)/\sigma_r^2$, where σ_r, σ_θ, and σ_ϕ are the radial, zenithal, and azimuthal velocity dispersions, respectively. One is the isotropic model of $\beta = 0$, which acts as our standard model. The other is the radially anisotropic model characterized by $\beta = 0.5$. This anisotropic model is motivated by the results of cosmological N-body simulations (Diemand et al. 2004; Abadi et al. 2006), which show an increase of β with r, starting $\beta \sim 0$ at a halo center to $\beta \gtrsim 0.5$ in its outer parts. For the sake of simplicity, we assume β is constant along r in our model.

2.2.2. Effect of baryon condensation

In hierarchical galaxy formation models, stars are formed by the condensation of cooled baryons at a halo center, subsequently forming a disk component. The condensed baryons or disk pulls the surrounding dark-matter particles inward, thereby increasing the central concentration of a dark halo (e.g., Gnedin et al. 2004). This effect of baryon condensation is also expected to modify the space and velocity distributions of subhalos, compared with those obtained by dissipationless N-body simulations (Gao et al. 2004).

We took into account this effect in our model by slowly increasing the total masses of the disk and bulge components over a period of 10 Gyr, after setting the initial distribution of subhalos in the presence of a (smooth) halo alone. When the total masses of the disk and bulge components reached the values listed in table 1, the position and velocity of each subhalo were recorded for use in further calculations of disk heating. In this experiment, we treated a subhalo as a point mass and neglected the interaction between different subhalos.

This treatment of the baryon condensation effect is admittedly highly ideal and not self-consistent, because we neglected the simultaneous modification for a smooth halo component.[1] However, the rate of the interactions between subhalos and a disk is somewhat increased by this gravitational effect of baryonic matter, thereby allowing us to carry out a statistically meaningful analysis on the properties of the disk heating. In fact, this effect of baryon condensation resulted in a few percent increase in the number of subhalos having pericenters smaller than ~ 10 kpc, which yielded a sufficient amount of interaction events over the interval of numerical simulations.

2.2.3. Internal density distribution

We considered two different models for the internal density distribution of a subhalo: point-mass and extended-mass models. In the former models, since point-mass subhalos survive eternally in our simulations, it was postulated that subhalos are supplied through their continuous accretion into a host halo from outside, even if some of them disappear due to tidal destruction. In the latter models affected by tides, we assumed a King-model profile, characterized by a concentration parameter, $c_{\rm King} = \log_{10}(R_{\rm t}/R_{\rm c})$, where $R_{\rm t}$ and $R_{\rm c}$ denote tidal and core radii, respectively. For these latter models, the tidal effects of the disk (as well as the bulge and halo) on subhalos are explicitly taken into account. While the adoption of a King-model profile is admittedly ideal, recent cosmological simulations by Kazantzidis et al. (2004) imply that the internal density distributions of subhalos may be described reasonably well by a more-centrally concentrated universal profile or the NFW profile with some tidal outer limit. We therefore adjusted our King models to match the NFW profile in the following manner. Firstly, based on the method outlined in NFW, we determined a set of model parameters in the NFW profile (see appendix 1 for details). Secondly, we estimated a parameter, $c_{\rm King}$, whereby the half-mass radius of the King

[1] Our adoption of an isothermal-like profile for a smooth halo [equation (3)], in comparison with an NFW-like profile derived from N-body simulations, suggests the consideration of baryon condensation for the halo setting.

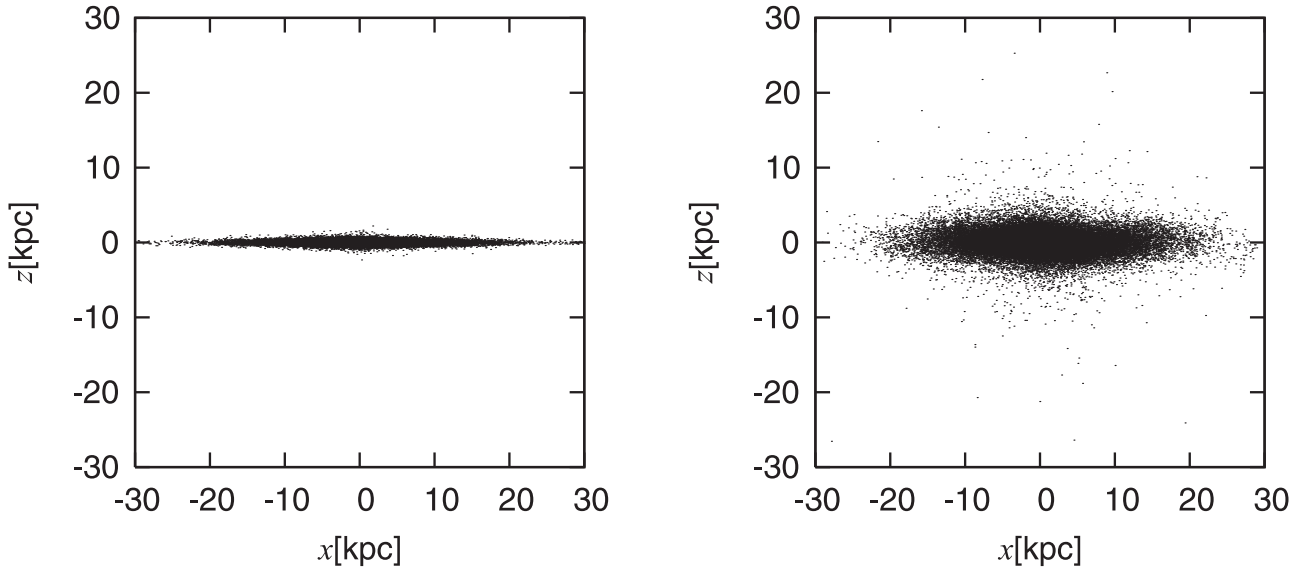

Fig. 3. Growth of the disk thickness for Model F. The left and right panels show edge-on views of the disk at the beginning ($t = 0$) and the end ($t = 4.9$ Gyr) of the simulation, respectively.

model would be equal to that of the NFW model. Finally, we obtained a tidal radius, R_t, as a limiting radius of the tidal effect of a host galaxy at the initial position of a subhalo. Thus, R_t is derived from the relation

$$\frac{M_{\rm tot}(< r)}{r^3} = \frac{M_{\rm sub}}{R_t^3}, \tag{6}$$

where $M_{\rm tot}(< r)$ is the total mass of a host galaxy interior to r and $M_{\rm sub}(< R_t)$ is the mass of a subhalo. For this estimation of R_t, we assumed a spherically symmetric potential for a host galaxy, where the disk is made spherical with a mass distribution $M_d(r) = M_d[1 - (1 + r/R_d)\exp(-r/R_d)]$. We also took into account the effects of baryon condensation for getting the initial position of a subhalo.

The parameters for point-mass models and extended-mass models that we calculated are summarized in table 2.

2.3. Method for Numerical Simulation

For the point-mass models we used a tree algorithm with a tolerance parameter of $\theta_{\rm tor} = 0.7$ (Barnes, Hut 1986; Hernquist 1987). For the extended-mass models we used GRAPE5 systems at the National Astronomical Observatory of Japan. The time integration was made with the leapfrog method and a fixed time step of 0.41 Myr. The softening length for N-body particles was $\epsilon = 70$ pc. We used $N_d = 46000$ particles for the disk; the numbers of subhalo particles are listed in table 2. Since the mass of the subhalo is negligibly small as compared with that of the host galaxy, we neglected the forces between the subhalos in the point-mass models. In contrast, for the extended-mass models, we fully took into account the gravitational interaction between the subhalos for the convenience of numerical calculations using GRAPE5. We followed the evolution for up to 4.9 Gyr.

3. Results

Based on numerical simulations of the models defined in the previous section, we now examine the effects of subhalos on the disk structure and dynamics, especially to elucidate the dependence of several different properties of subhalos: their internal density distribution, mass function, and spatial and velocity distributions.

In figure 3 we show an edge-on view of the disk for Model F at the beginning ($t = 0$) and the end ($t = 4.9$ Gyr) of the simulation. The disk has been thickened and tilted by the gravitational interaction with orbiting subhalos. To estimate the change of the disk kinematics and thickness at specific locations, we consider the tilt of the disk and use the axes aligned with the principal axes of the disk inertia tensor. The heating and thickening of the disk can be described by the changes of the velocity dispersions ($\Delta\sigma_R$, $\Delta\sigma_z$) and by the increase of the scale height, Δz_d. To calculate these quantities, the disk was stratified in concentric cylindrical annuli with a width of $\delta R = 700$ pc and the particle properties were averaged in each annulus. The scale height in each annulus R of the disk, z_d, is defined by the mean square of the z-coordinates, i.e., $z_d(R) \equiv \langle z^2 \rangle^{1/2}$. We note that at the beginning of the calculations, z_d was a constant of 245 pc, as given in equation (1).

In addition to the dynamical effect of subhalos, the simulated disk is subject to internal heating due to two-body relaxation among the disk particles; this numerical heating always took place in numerical simulations with a modest number of particles. We evaluated the effect of internal heating by evolving the disk in isolation, i.e., in the absence of subhalos. This effect is typically characterized as $\Delta z_d = 0.23$ kpc, $\Delta\sigma_R = 7.2\,{\rm km\,s^{-1}}$, and $\Delta\sigma_z = 5.7\,{\rm km\,s^{-1}}$ at the solar radius after 4.9 Gyr. In the following, the notation Δz_d means the difference of a scale height between $t = 4.9$ Gyr and $t = 0$, and $\Delta\sigma_R$ and $\Delta\sigma_z$ also mean the change of the velocity dispersions after 4.9 Gyr.

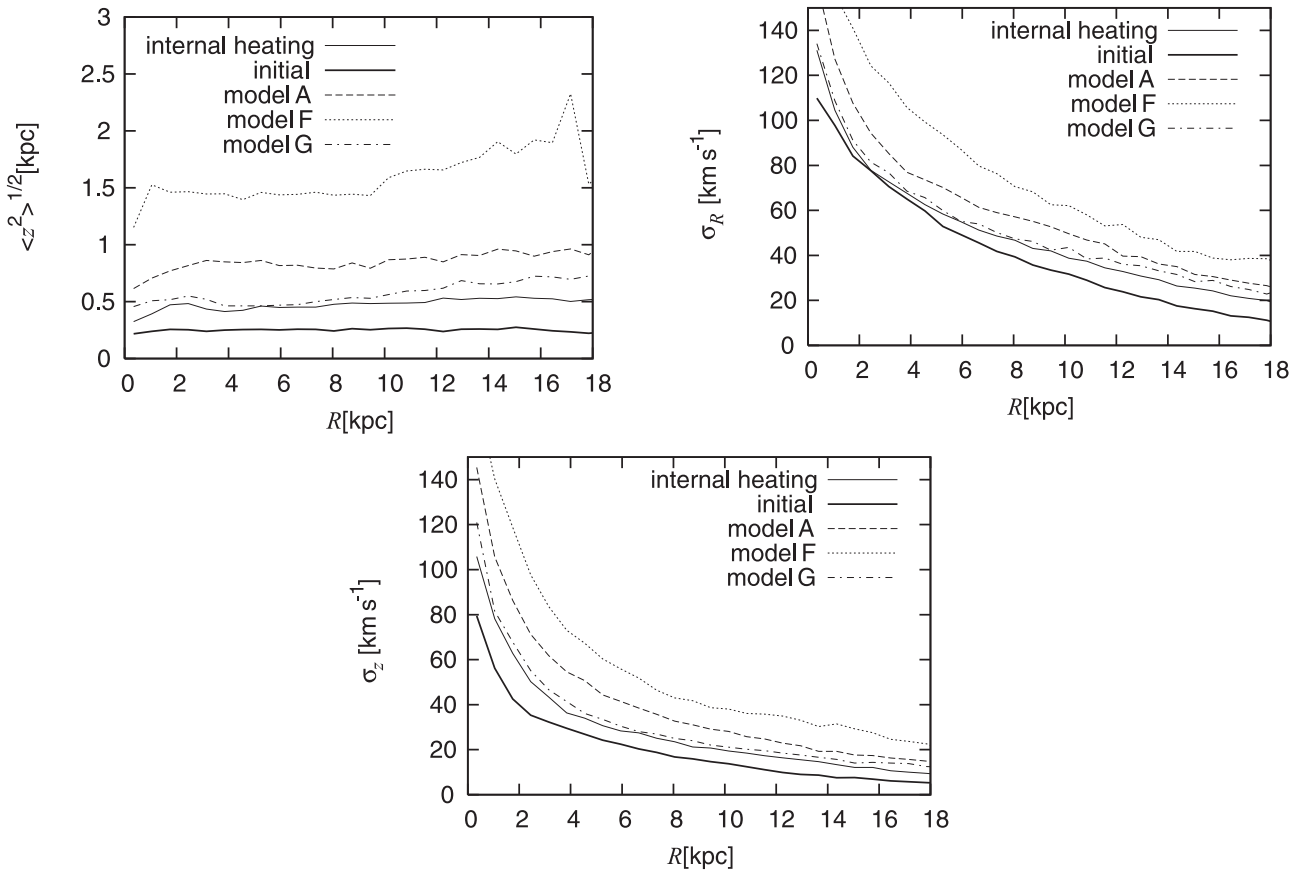

Fig. 4. Kinematical properties of the disk after 4.9 Gyr for different subhalo models. The thick solid lines show the initial setting and the thin solid lines show the effects of internal heating in the absence of subhalos. The dashed, dotted, and dash-dotted lines show Models A, F, and G, respectively.

3.1. Global Properties of the Disk Evolution

Figure 4 shows the kinematical properties of the disk for Models A, F, and G, including the impact of internal heating in our calculations. It is evident from this figure that thickening of the disk does not occur uniformly at all radii; given the complexity of the final disk structure, we found it convenient to sample the kinematics at $R = R_\odot$, $3\,R_\mathrm{d}$, and $4\,R_\mathrm{d}$, which was sufficient to provide us with a global view of the heating and thickening. The growth of the disk thickness in Model A is $\Delta z_\mathrm{d} \sim 0.57$ kpc, 0.61 kpc, and 0.67 kpc at $R = R_\odot$, $3\,R_\mathrm{d}$, and $4\,R_\mathrm{d}$, respectively, those values in Model F are 1.19 kpc, 1.37 kpc, and 1.60 kpc, and those values in Model G are 0.28 kpc, 0.31 kpc, and 0.39 kpc. The increase in the radial and vertical velocity dispersions after 4.9 Gyr in Model A is given as $(\Delta\sigma_R, \Delta\sigma_z) = (18.8, 15.4)$, (17.4, 13.8), and (16.6, 11.9) km s^{-1} at $R = R_\odot$, $3\,R_\mathrm{d}$, and $4\,R_\mathrm{d}$, respectively, those values in Model F are (32.2, 26.1), (30.1, 23.9), and (25.4, 22.8) km s^{-1}, and those values in Model G are (9.9, 8.2), (10.5, 7.5), and (13.5, 8.2) km s^{-1}.

In these experiments, the main difference between Model A and Model F resides in the individual masses of subhalos, parameterized by M_high and M_low (see table 2): for Model A all subhalos have $10^8\,M_\odot$ as $M_\mathrm{high} = M_\mathrm{low} = 10^8\,M_\odot$, whereas for Model F the presence of more massive subhalos than $10^8\,M_\odot$ is allowed as $M_\mathrm{high} = 10^9\,M_\odot$. Therefore, a comparison between the results of these two models highlights the effect of individual masses of subhalos on the disk heating, where we note that a slight difference in parameter a between the models by a factor 1.25 yields essentially no difference in the results. It is clear that the presence of a few, but massive, subhalos (Model F) is more effective for disk heating than the case of many, but less massive ones (Model A), as already pointed out by Ardi et al. (2003). This suggests that the disk heating process is more sensitively enhanced than being proportional to individual subhalo masses; massive subhalos are more important for disk heating. Also, compared with Model F, Model G with the same values for M_high and M_low yields a weak effect on the disk. The main difference between these two models is the spatial distribution of subhalos, parameterized by a (a = 87.5 kpc and 280 kpc for Models F and G, respectively), which affects the pericenter distributions of subhalos, especially at $r \lesssim 10$ kpc (see figure 2). Therefore, we find that the number of subhalos crossing the disk is also important in quantifying the disk heating.

Figure 5 shows the growth of the disk velocity dispersions in the radial and vertical directions at $R = R_\odot$ for Models F (the point-mass model), K, and L (the extended-mass model). This figure shows that the disk velocity dispersion for Model F continues to grow throughout the simulations, whereas for Models K and L the growth of the velocity dispersion almost stops at $t \sim 1$ Gyr. It is worth noting that in these latter models

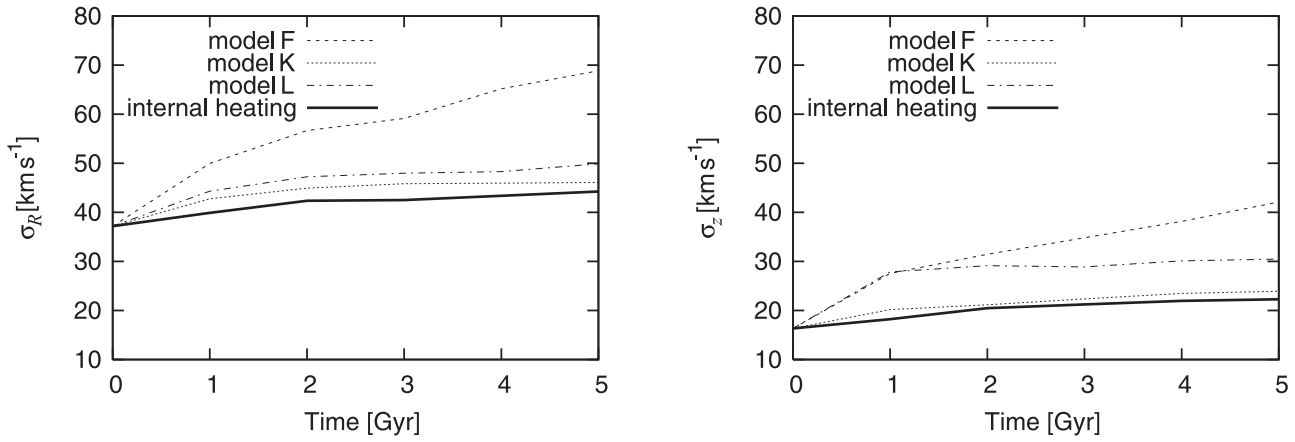

Fig. 5. Growth of the disk velocity dispersion in the radial and vertical directions at $R = R_\odot$ for Models F (dashed lines), K (dotted lines), and L (dash-dotted lines). In Model F subhalos are represented by point masses, whereas in Models K and L they have a King-model profile. The thick solid lines show the effect of internal heating in the absence of subhalos.

subhalos can lose their mass at the interaction with the disk, unlike the former point-mass models in which subhalo masses remain the same. Thus, for the extended-mass models the effect of subhalos on the disk is temporal; subhalos appear to lose almost all of their mass at the first interaction with the disk, so that their role in the disk heating is effective only at the first interaction with the disk.

3.2. Disk Thickness vs. Subhalo Masses

In this section we consider in more detail the effect of orbiting subhalos on the growth of the disk thickness. As discussed above, the change in the disk scale height, z_d, depends on R, in such a manner that Δz_d is somewhat larger at larger R. To quantify this disk thickening as a function of the accreted subhalo masses, we utilize the disk scale height at the outer edge of the disk, $R = R_{out}$, where the stellar light distribution is expected to diminish steeply with R. This truncation of a stellar disk has actually been observed, where the stellar light declines more steeply than an exponential profile for a main disk, and drops to low values beyond the so-called truncation radius (van der Kruit, Searle 1981a, b, 1982; Kregel et al. 2002). This usually occurs at a radius of 3–5 disk scale length (Kregel et al. 2002), so in our work we adopt $R_{out} = 3\,R_d$ as a characteristic outer edge of the disk, at which the change of the disk scale height is evaluated. Also, to analyze the relation between the change of the disk thickness and the orbits of the accreted subhalos, we estimate the number of times that each subhalo crosses the disk region at $R \leq 3\,R_d$ during the course of its orbital motion.

We carried out simulations for several different models of point-mass subhalos with $\beta = 0$. Figure 6 shows the relation between the growth of the disk scale height at $R = 3\,R_d$ (i.e. $\Delta z_d/R_d$) and the combination of each mass of a subhalo, $M_{sub,i}$, and the number of times that it crosses the disk at $R \leq 3\,R_d$ during the course of its orbital motion, denoted as N_i [i.e. $\sum_i N_i(M_{sub,i}/M_d)$ for the left panel and $\sum_i N_i(M_{sub,i}/M_d)^2$ for the right panel]. Here, the abscissa for the left panel is proportional to the total accreted mass of subhalos, whereas that for the right panel is proportional to the sum of the squared masses of subhalos. As is evident, while the left panel shows no correlation between the abscissa and ordinate axes, the right panel shows a significantly tight correlation, thereby indicating that the growth of the disk thickness is proportional to the sum of the squared masses of the subhalos; if so, the disk thickening is more enhanced for more massive individual subhalos, as already shown in the previous subsection. We thus investigated this relation for different subhalo models, as shown in figure 7. In the left panel we consider the extended-mass models with $\beta = 0$ (filled squares) compared with the point-mass models with $\beta = 0$ (open circles). We note here that in the extended-mass models subhalos lose almost all of their mass at the first interaction with the disk, so we adopted $N_i = 1$ for such a case. The right panel shows the case of an anisotropic velocity distribution with $\beta = 0.5$ for the point-mass models (filled triangles) and with $\beta = 0$ for the point-mass models (open circles). As is evident from these panels, several different models yield an almost universal relation between $\Delta z_d/R_d$ at $R = 3\,R_d$ and $\sum_i N_i(M_{sub,i}/M_d)^2$ at $R \leq 3\,R_d$.

4. Discussion

4.1. Dependence of Disk Heating on Subhalo Masses

From the results of subsection 3.2, we find that the disk thickness increases with the accretion of subhalos into a disk. Our numerical experiments suggest the following universal relation:

$$\frac{\Delta z_d}{R_d} = \alpha \sum_i N_i \left(\frac{M_{sub,i}}{M_d}\right)^2, \tag{7}$$

where α is a constant of $\simeq 8$, R_d is the disk scale length, z_d is the disk scale height at $R = 3\,R_d$, and N_i is the number of times that subhalos with an individual mass of $M_{sub,i}$ cross a disk at $R \leq 3\,R_d$ (noting that $N_i = 1$ for the extended-mass models as subhalos lose their mass at their first interaction with the disk). In this expression, subscript i denotes an individual subhalo given at $t = 0$ in our simulation. An alternative, more useful expression based on equation (7) is

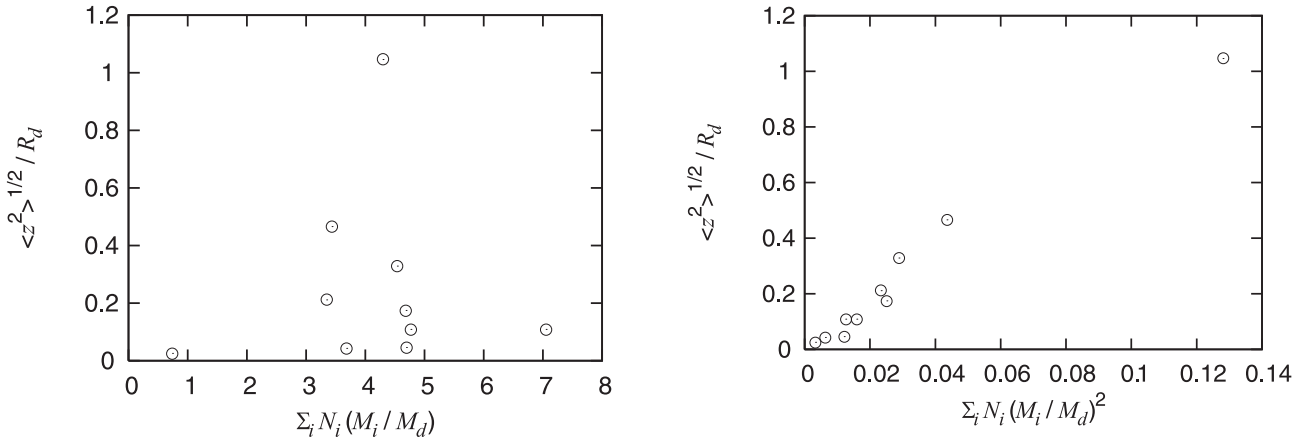

Fig. 6. Relation between the growth of the disk scale height at $R = 3\,R_{\rm d}$ and the combination of each mass of a subhalo $M_{{\rm sub},i}$ and the number of times that it crosses the disk at $R \leq 3\,R_{\rm d}$, denoted as N_i, for the point-mass subhalo models with $\beta = 0$ (Models A to J listed in table 2). The abscissas in the left and right panels show $\sum_i N_i (M_{{\rm sub},i}/M_{\rm d})$ and $\sum_i N_i (M_{{\rm sub},i}/M_{\rm d})^2$, respectively. Notice that the effect of internal heating has been subtracted in these plots.

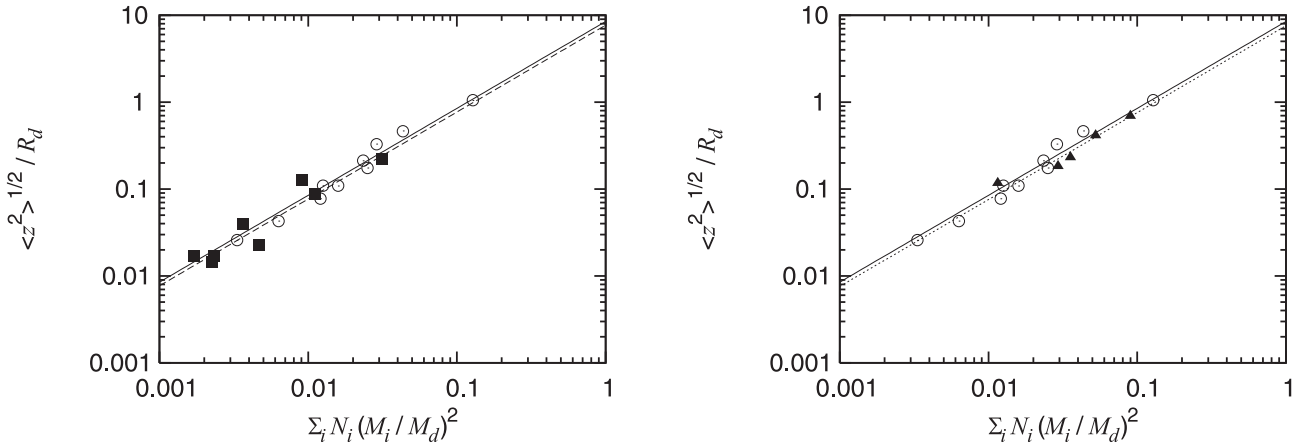

Fig. 7. Same as figure 6, but for several different subhalo models plotted on logarithmic scales. The left panel shows the extended-mass models with $\beta = 0$ (filled squares) compared with the point-mass models with $\beta = 0$ (open circles), whereas the right panel shows the case of an anisotropic velocity distribution with $\beta = 0.5$ for the point-mass models (filled triangles) and point-mass models with $\beta = 0$ (open circles). The solid lines show the fitting to the relations for the point-mass models with $\beta = 0$ by the least-squares method, dashed lines for the extended-mass models with $\beta = 0$, and dotted lines for the point-mass models with $\beta = 0.5$.

derived as follows. Supposing that the disk has experienced the accretion of subhalos having an individual mass of $M_{{\rm sub},j}$ with $j = 1, \ldots, N$ at $R \leq 3\,R_{\rm d}$, where the repeated accretion of a subhalo in the course of its orbital motion is regarded as a separate accretion event with a mass $M_{{\rm sub},j}$, and N denotes the total number of such events. Then, we obtain the relation

$$\frac{\Delta z_{\rm d}}{R_{\rm d}} \simeq 8 \sum_{j=1}^{N} \left(\frac{M_{{\rm sub},j}}{M_{\rm d}} \right)^2, \tag{8}$$

which holds a more useful form for any applications than equation (7). Notice that although this relation is derived from simulations over the interval of 4.9 Gyr, this is applicable to longer time evolution by considering the total number of subhalos crossing a disk, N.

As equation (8) indicates, the increase of the disk thickness is proportional to the square of the masses of accreted subhalos. This mass dependency in the disk heating process can be understood if we consider the transfer of kinetic energy from the subhalos to the disk through dynamical friction. Here, we present a summary of this derivation; more details are given in appendix 2.

Firstly, the vertical equilibrium between the kinetic and gravitational energy allows us to relate the velocity dispersion, σ_z, and the scale height, $z_{\rm d}$, of a disk. Assuming that a disk is an isothermal sheet, we obtain

$$\sigma_z^2 = 2\pi G\, \Sigma(R)\, z_{\rm d}, \tag{9}$$

where $\Sigma(R)$ is a surface density of a disk at R (e.g. Spitzer 1942). Secondly, we consider the energy input into disk stars getting through subhalo–disk interaction: the energy loss of a subhalo is equal to the energy pumped into a disk. This energy loss, $\Delta E_{\rm sub}$, is derived by the integral over an orbit of a subhalo,

$$\Delta E_{\rm sub} = \int F_{\rm drag}\, ds, \tag{10}$$

where $F_{\rm drag}$ corresponds to the dynamical friction. Using the Chandrasekhar formula for $F_{\rm drag}$, each subhalo with mass $M_{\rm sub}$ is subject to a frictional force with $F_{\rm drag} \propto M_{\rm sub}^2$. Finally, combining equation (9) with (10), we obtain

$$\Delta z_{\rm d} \propto \Delta\sigma_z^2 \propto \Delta E_{\rm sub} \sim F_{\rm drag} \cdot z_{\rm d} \propto M_{\rm sub}^2. \tag{11}$$

Therefore, the dependence of $\Delta z_{\rm d}$ on $M_{\rm sub}$, as discussed in section 3, is understood within the framework of dynamical friction between a subhalo and a disk.

4.2. Comparison with an Observed Thin Disk

Recent observations of external disk galaxies by Kregel et al. (2002) have suggested that the thickness of a (thin) disk is confined to some limiting value relative to the scale length of a disk, which is expressed as $z_{\rm d}/R_{\rm d} < 0.2$. Kregel et al. (2002) have also shown that the distribution of $z_{\rm d}/R_{\rm d}$ tends to have an increasing dispersion with increasing maximum circular velocity, $V_{\rm c}$, of a disk, in such a manner that a larger $V_{\rm c}$ allows a smaller $z_{\rm d}/R_{\rm d}$; conversely, a disk with a smaller $V_{\rm c}$ is likely to be thicker.

An observed thin disk with $z_{\rm d}/R_{\rm d} < 0.2$ suggests that the accretion of subhalos has been rather insignificant, since a disk with a current mass was formed. Using equation (8), this observed limit implies $\left(\sum_j M_{{\rm sub},j}^2\right)^{1/2} < 0.15\, M_{\rm d}$. Thus, we find that an observed thin disk has not ever interacted with subhalos with a total mass of more than 15% of the disk mass.

The dependence of $z_{\rm d}/R_{\rm d}$ on $V_{\rm c}$ may be understood as follows. Let $\langle M_{\rm sub}^2\rangle$ be the mean square of a subhalo mass, defined as $\langle M_{\rm sub}^2\rangle = \sum_j^N M_{{\rm sub},j}^2/N$. Then, equation (8) can be written as

$$\frac{\Delta z_{\rm d}}{R_{\rm d}} \propto N \frac{\langle M_{\rm sub}^2\rangle}{M_{\rm d}^2}. \tag{12}$$

We suppose that N, the number of subhalos that cross a disk at $R \le 3\,R_{\rm d}$, is roughly proportional to the spherical volume with radius $3\,R_{\rm d}$ inside a dark halo, given the spatial distribution of subhalos. This reads $N \propto R_{\rm d}^3$. Also suppose that the central disk surface density, $\Sigma_0 = M_{\rm d}/(2\pi R_{\rm d}^2)$, is nearly the same for a disk galaxy, which may correspond to nearly the same central surface brightness for a bright disk (e.g., Freeman 1970). Then equation (12) is rewritten as

$$\frac{\Delta z_{\rm d}}{R_{\rm d}} \propto \langle M_{\rm sub}^2\rangle \cdot V_{\rm c}^{-2}, \tag{13}$$

where $V_{\rm c}$ is the disk circular velocity derived from $V_{\rm c}^2 \propto G M_{\rm d}/R_{\rm d}$.

Thus, if the observed disk thickness is controlled by disk-subhalo interaction, i.e., $z_{\rm d} \sim \Delta z_{\rm d}$, and $\langle M_{\rm sub}^2\rangle$ is roughly the same for each disk galaxy, we find that the effect of subhalos on a disk with a smaller mass is more significant than a disk with a larger mass. This is in good agreement with the observation (Kregel et al. 2002) that a disk with smaller $V_{\rm c}$ is likely to be thicker.

4.3. Relation to the Origin of a Thick Disk

In recent years, new datasets for the thick-disk component of the Galaxy as well as for a thick disk of an external galaxy have been available, showing several important properties of a thick disk. Based on the third data release of the Sloan Digital Sky Survey (York et al. 2000), Allende Prieto et al. (2006) found that stars belonging to the thick disk have no vertical metallicity gradient. The rotational velocity for the same stars, however, shows a vertical gradient of $\sim -16\,{\rm km\,s^{-1}\,kpc^{-1}}$ between 1 and 3 kpc from the Galactic plane. The observations of an external disk galaxy (Yoachim, Dalcanton 2006) have shown that the ratio of the total luminosity of a thick disk to that of a thin one is related to the circular velocity of a galaxy, in such a manner that the ratio tends to increase with decreasing circular velocity; a less massive galaxy has a brighter (and possibly more massive) thick disk relative to a thin one. These properties of a thick disk are expected to set important constraints on its origin.

Here, we consider the possibility that a thick disk has been formed by the dynamical effect of numerous dark subhalos on a pre-existing disk. This interaction effect may be rather weak at the current epoch, because only a small fraction of subhalos would cross a disk (Font et al. 2001), but the effect at early times may have been more significant due to a smaller disk mass and larger accretion rate of subhalos onto a parent halo. If so, a pre-existing disk should have suffered from considerable heating at early times, which would result in the formation of a thick disk; subsequent slow accumulation of baryonic gas in a plane may form a thin-disk component.

To assess this possibility in light of the observed properties of a thick disk, we investigated the properties of a disk thickened by subhalos in our model. Figure 8 shows the distribution of the stars in Model F at the end of the simulation ($t = 4.9$ Gyr), differentiated by the initial ($t = 0$) positions at either $z < 245$ pc (left panel) or $z > 245$ pc (right panel). As is evident, the disk stars are well mixed by disk heating. This suggests that even if a pre-existing disk had a metallicity gradient, the disk heating by interactions with subhalos would have wiped out this gradient, leaving a thick disk, in agreement with observations. It is also suggested that this disk heating process prompts a vertical gradient in rotational velocity. This is explained as follows. A heated disk puffs up not only in the vertical, but also in the radial direction, where the stars located at high $|z|$ have a large radial velocity dispersion compared with those at low $|z|$, and thus have small rotational velocities on average due to the effect of asymmetric drift; given a gravitational force inward, the increase of radial pressure of stars reduces the effect of the centrifugal force. This vertical gradient in rotational velocity was actually obtained in our simulation models, as shown in figure 9. It was found that the gradient amounts to $-(10$–$30)\,{\rm km\,s^{-1}\,kpc^{-1}}$ between 1 and 3 kpc from the plane, in good agreement with the observations. This experiment suggests that the presence of a vertical gradient in rotational velocity of a thick disk may be an important clue to distinguishing the scenarios for the origin of a thick disk; models invoking monolithic disk collapse (Burkert et al. 1992) or a chaotic merging event of building blocks (Brook et al. 2004) at early times of a galaxy may have difficulties in this regard.

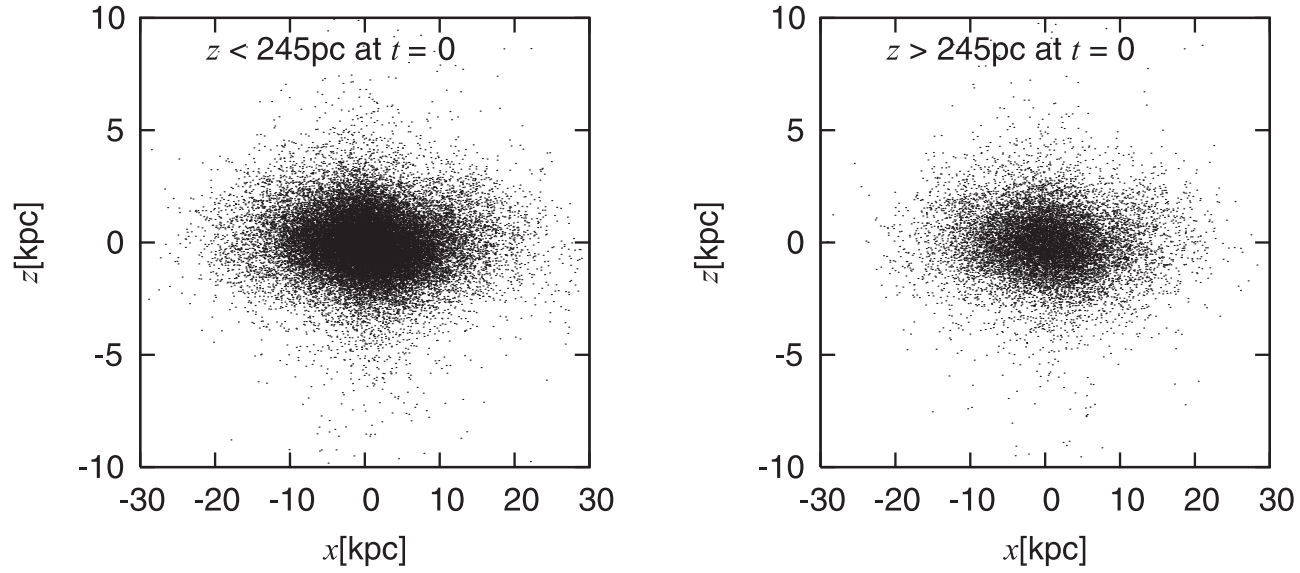

Fig. 8. Distribution of stars in Model F at the end of the simulation ($t = 4.9$ Gyr), differentiated by their initial ($t = 0$) positions at $z < 245$ pc (left panel) and $z > 245$ pc (right panel).

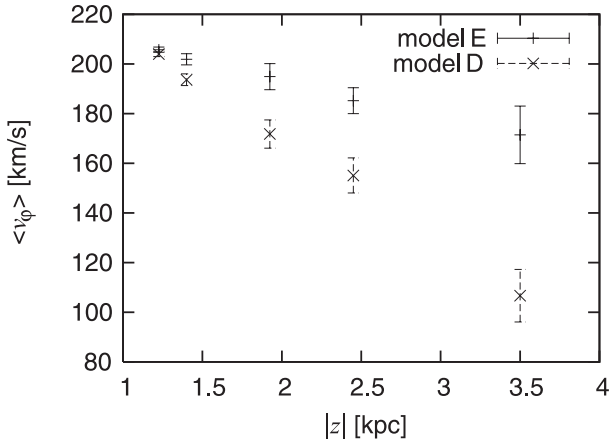

Fig. 9. Mean azimuthal velocity of the stars located at annulus $R = R_\odot \pm 1.05$ kpc as a function of the distance away from the plane, for Models D and E. Note that both models show a similar vertical scale height, $z_d \approx 1$ kpc, at the end of the simulations ($t = 4.9$ Gyr).

A more definite picture for the formation of a thick disk must await more elaborate modeling of a forming galaxy in the context of hierarchical clustering. In particular, each galaxy has a different merging history of subhalos, and so different spatial and velocity distributions, which inevitably affect the interpretation for the observed properties of a thick disk, such as for its fraction as a function of a disk mass. Also, observations show that almost all of the disk galaxies have a distinct thick disk in addition to a thin component. This implies that the dynamical effects of subhalos on a disk are significant only before a specific epoch, and the subsequent formation of a thin disk is unaffected by subhalos, although it is yet unclear if this is applicable to all galaxy-sized halos having different merging histories. Therefore, to assess the scenario, more detailed numerical studies are required that take into account the growth of both a dark halo and a disk simultaneously.

5. Conclusions

We summarize our conclusions as follows:

- The dynamical effects of subhalos on a disk are represented by the relation between the change of the disk scale height, Δz_d (measured at the disk edge $R = 3\,R_d$) and the individual masses of subhalos, M_{sub}, i.e., $\Delta z_d/R_d \simeq 8\sum_{j=1}^{N}(M_{sub,j}/M_d)^2$, where R_d is the disk scale length, M_d is the disk mass, and N is the total number of accretion events of subhalos inside a disk region ($\leq 3\,R_d$).
- If subhalos with a total mass of more than 15% of the disk mass interact with a disk, then the disk thickness is made larger than the observed range.
- A less-massive disk with a smaller circular velocity, V_c, is found to be more affected by subhalos than a disk with larger V_c, which is in agreement with the observed properties of a thin disk.
- Stars in a significantly thickened disk by subhalos appear to be well mixed, and show a vertical gradient in their rotation velocity, being similar to the observed properties of thick disks in the Galaxy.

We note that relation (8) obtained here is universal, and is thus useful for applications to any relevant issues, including the dynamics of an evolving stellar disk at the center of a growing dark halo. Such detailed studies of a galactic disk compared with recently increasing datasets of a remote disk galaxy will be of great importance, and is left to future work.

The numerical computations reported here were carried out on GRAPE systems (project ID: g05b05) kindly made available by the Astronomical Data Analysis Center (ADAC) at the National Astronomical Observatory of Japan (NAOJ).

This work has been supported in part by a Grant-in-Aid for Scientific Research (15540241, 17540210) from the Ministry of Education, Culture, Sports, Science and Technology.

Appendix 1. NFW Profile

The NFW density profile is given by

$$\rho = \rho_{\rm crit} \frac{\delta_0}{(r/r_{\rm s})(1 + r/r_{\rm s})^2}, \tag{A1}$$

where $\rho_{\rm crit}$ is the critical density of the Universe, $r_{\rm s}$ is a scale radius, and δ_0 is the characteristic density contrast. Following NFW, we define the limiting radius of a virialized halo, r_{200}, to be the radius within which the mean mass density is $200\,\rho_{\rm crit}$. Also, the concentration parameter of a halo is defined as $c = r_{200}/r_{\rm s}$, with which δ_0 is given as

$$\delta_0 = \frac{200}{3} \frac{c^3}{[\ln(1 + c) - c/(1 + c)]}. \tag{A2}$$

To put the NFW density profile in a cosmological context, we need to calculate the concentration factor, c, which is related to δ_0 via equation (A2). The appropriate value of c depends on halo formation history and on cosmology. NFW proposed a simple model for c based on halo formation time. The formation redshift, $z_{\rm coll}$, of a halo identified at $z = 0$ with mass M is defined as the redshift by which half of its mass is in progenitors with the mass exceeding fM, where f is a constant. With this definition, $z_{\rm coll}$ can be computed by simply using the Press–Schechter formalism (e.g. Lacey, Cole 1993),

$$\mathrm{erf}\left\{ \frac{\delta_{\rm c}(z_{\rm coll}) - \delta_{\rm c}^0}{\sqrt{2[\Delta_0^2(fM) - \Delta_0^2(M)]}} \right\} = \frac{1}{2}, \tag{A3}$$

where $\Delta_0^2(M)$ is the linear variance of the power spectrum at $z = 0$ smoothed with a top-hat filter of mass M, $\delta_{\rm c}(z)$ is the density threshold for spherical collapse by redshift z, and $\delta_{\rm c}^0 = \delta_{\rm c}(0)$. NFW found that the characteristic overdensity of a halo at $z = 0$ is related to its formation redshift, $z_{\rm coll}$, by

$$\delta_0(M, f) = C(f)\Omega_0[1 + z_{\rm coll}(M, f)]^2, \tag{A4}$$

where the normalization $C(f)$ depends on f and Ω_0 is the current density parameter of the Universe. We take $f = 0.01$, as suggested by the N-body results of NFW. In this case $C(f) \approx 3 \times 10^3$. Thus, for a halo of given mass at $z = 0$, one can obtain the concentration factor c from equations (A2)–(A4). In practice, we first solve $z_{\rm coll}$ from equation (A3) and insert the value of $z_{\rm coll}$ into equation (A4) to get δ_0. We then use this value of δ_0 in equation (A2) to solve for c.

In this experiment, we adopted a standard set of cosmological parameters as $\Omega_0 = 0.3$, $\Lambda = 0.7$, $h = 0.7$, and $\sigma_8 = 1.3$, where Λ is the cosmological constant, h is the normalized Hubble constant of $h \equiv H_0/100\,{\rm km\,s^{-1}\,Mpc^{-1}}$, and σ_8 parameterizes density fluctuations at $8\,h^{-1}\,$Mpc.

Appendix 2. Derivation of Equation (8)

We show here the derivation of equation (8) based on the following dimensional analysis.

Firstly, we derive the relation between the vertical velocity dispersion, σ_z, of disk stars and the scale height, $z_{\rm d}$, of a self-gravitating axisymmetric disk in cylindrical coordinates (R, z). For the limit of a thin disk where z-derivatives dominate over R-derivatives, an equation for the vertical equilibrium and the Poisson equation read, respectively,

$$\frac{1}{\rho_{\rm d}} \frac{\partial(\rho_{\rm d}\sigma_z^2)}{\partial z} + \frac{\partial \Phi}{\partial z} \simeq 0, \quad \frac{\partial^2 \Phi}{\partial z^2} \simeq 4\pi G\rho, \tag{A5}$$

where $\rho_{\rm d}$ is a mass density of a disk and Φ is a gravitational potential. Integrating the second equation over all z gives the surface mass density $\Sigma(R)$ vs. Φ, i.e., $2\pi G\Sigma(R) \simeq \partial\Phi/\partial z$. Then, inserting this into the first equation, and assuming $\rho_{\rm d} \propto \exp(-z/z_{\rm d})$ and σ_z is constant, we obtain $z_{\rm d} \simeq \sigma_z^2/[2\pi G\Sigma(R)]$. This equation suggests that the change in the disk thickness is related to the change in the velocity dispersion, i.e.,

$$\Delta z_{\rm d} \simeq \frac{\Delta\sigma_z^2}{2\pi G\,\Sigma(R)}. \tag{A6}$$

Secondly, the change in the velocity dispersion, $\Delta\sigma_z^2$, is related to the energy input into disk stars getting through subhalo–disk interaction: the energy loss of a subhalo is equal to the energy pumped into a disk. Denoting this energy loss as $\Delta E_{\rm sub}$ per a subhalo, the resultant $\Delta\sigma_z^2$ for a disk with a total mass, $M_{\rm d}$, reads

$$\Delta\sigma_z^2 = \frac{2\Delta E_{\rm sub}}{M_{\rm d}}. \tag{A7}$$

We note that $\Delta E_{\rm sub}$ is derived by the integral over an orbit of a subhalo,

$$\Delta E_{\rm sub} = \int F_{\rm drag}\, ds \sim F_{\rm drag}\, z_{\rm d}, \tag{A8}$$

where $F_{\rm drag}$ corresponds to a dynamical friction. Using the Chandrasekhar formula for $F_{\rm drag}$, each subhalo with mass $M_{\rm sub}$ is subject to a frictional force with

$$F_{\rm drag} = \frac{4\pi G^2 M_{\rm sub}^2 \rho_{\rm d} \ln\Lambda}{v_{\rm sub}^2} \left[\mathrm{erf}(X) - \frac{2X}{\sqrt{\pi}} e^{-X^2} \right], \tag{A9}$$

where $\ln\Lambda$ is the Coulomb logarithm, $X \equiv v_{\rm sub}/(\sqrt{2}\sigma)$ with σ being the disk velocity dispersion, and $v_{\rm sub}$ is the subhalo's velocity. For $v_{\rm sub}$, we suppose that it is represented by the virial velocity of a smooth dark halo with mass $M_{\rm H}$ and radius $r_{\rm H}$, giving $v_{\rm sub}^2 \sim GM_{\rm H}/r_{\rm H}$. Furthermore, if $M_{\rm d}$ and $R_{\rm d}$ for a disk is some fraction of $M_{\rm H}$ and $r_{\rm H}$, given as $M_{\rm d} = f_1 M_{\rm H}$ and $R_{\rm d} = f_2 r_{\rm H}$, where typically $f_1 \sim f_2 \sim O(10^{-1})$, we obtain $v_{\rm sub}^2 \sim GM_{\rm d}/R_{\rm d}$. For $\rho_{\rm d}$, we set $\rho_{\rm d} \sim M_{\rm d}/(R_{\rm d}^2 z_{\rm d})$.

Finally, using the above equations, the change in the disk thickness induced by N accretion events of subhalos is estimated by

$$\Delta z_{\rm d} \propto \frac{N\Delta\sigma_z^2}{G\Sigma} \propto \frac{NG^2 z_{\rm d} M_{\rm sub}^2 \rho_{\rm d}/v_{\rm sub}^2}{G\Sigma M_{\rm d}} \propto \frac{NM_{\rm sub}^2}{\Sigma M_{\rm d} R_{\rm d}}. \tag{A10}$$

Thus, we obtain

$$\frac{\Delta z_{\rm d}}{R_{\rm d}} \propto N \frac{M_{\rm sub}^2}{M_{\rm d}^2}, \tag{A11}$$

which is consistent with equation (8).

References

Abadi, M. G., Navarro, J. F., & Steinmetz, M. 2006, MNRAS, 365, 747

Allende Prieto, C., Beers, T. C., Wilhelm, R., Newberg, H. J., Rockosi, C. M., Yanny, B., & Lee, Y. S. 2006, ApJ, 636, 804

Ardi, E., Tsuchiya, T., & Burkert, A. 2003, ApJ, 596, 204

Barnes, J. E., & Hut, P. 1986, Nature, 324, 446

Brook, C. B., Kawata, D., Gibson, B. K., & Freeman, K. C. 2004, ApJ, 612, 894

Burkert, A., Truran, J. W., & Hensler, G. 1992, ApJ, 391, 651

Diemand, J., Moore, B., & Stadel, J. 2004, MNRAS, 352, 535

Font, A. S., Navarro, J. F., Stadel, J., & Quinn, T. 2001, ApJ, 563, L1

Freeman, K. C. 1970, ApJ, 160, 811

Gao, L., White, S. D. M., Jenkins, A., Stoehr, F., & Springel, V. 2004, MNRAS, 355, 819

Ghigna, S., Moore, B., Governato, F., Lake, G., Quinn, T., & Stadel, J. 2000, ApJ, 544, 616

Gnedin, O. Y., Kravtsov, A. V., Klypin, A. A., & Nagai, D. 2004, ApJ, 616, 16

Hernquist, L. 1987, ApJS, 64, 715

Hernquist, L. 1990, ApJ, 356, 359

Hernquist, L. 1993, ApJS, 86, 389

Kazantzidis, S., Mayer, L., Mastropietro, C., Diemand, J., Stadel, J., & Moore, B. 2004, ApJ, 608, 663

Klypin, A., Kravtsov, A. V., Valenzuela, O., & Prada, F. 1999, ApJ, 522, 82

Kregel, M., van der Kruit, P. C., & de Grijs, R. 2002, MNRAS, 334, 646

Lacey, C., & Cole, S. 1993, MNRAS, 262, 626

Moore, B., Ghigna, S., Governato, F., Lake, G., Quinn, T., Stadel, J., & Tozzi, P. 1999, ApJ, 524, L19

Navarro, J. F., Frenk, C. S., & White, S. D. M. 1997, ApJ, 490, 493 (NFW)

Spitzer, L., Jr. 1942, ApJ, 95, 329

Summers, F. J., Davis, M., & Evrard, A. E. 1995, ApJ, 454, 1

Tóth, G., & Ostriker, J. P. 1992, ApJ, 389, 5

van der Kruit, P. C., & Searle, L. 1981a, A&A, 95, 105

van der Kruit, P. C., & Searle, L. 1981b, A&A, 95, 116

van der Kruit, P. C., & Searle, L. 1982, A&A, 110, 61

Velázquez, H., & White, S. D. M. 1999, MNRAS, 304, 254

Yoachim, P., & Dalcanton, J. J. 2006, AJ, 131, 226

York, D. G., et al. 2000, AJ, 120, 1579